Comparing Seismic Resolution and Signal and Noise Quality between Dense Point-Receiver and Conventional Data, Bakken Formation, North Dakota*

Niranjan Banik[1], Antoun Salama[1], Adam Koesoemadinata[1], George El-Kaseeh[1], Mark Egan[1], and Alfonso Gonzalez[1]

Search and Discovery Article #41160 (2013)
Posted July 31, 2013

*Adapted from extended abstract prepared in conjunction with poster presentation at AAPG Annual Convention and Exhibition, Pittsburg, Pennsylvania, May 19-22, 2013,

[1]Schlumberger-WesternGeco, Houston, TX (nbanik@slb.com)

Abstract

Substantial vertical and spatial heterogeneities in reservoir and completion qualities are now recognized characteristics of shale reservoirs. This is especially true in the Bakken resource of the Williston Basin, North Dakota, in which the production comes from the thin Middle Bakken Formation. The lithology of the Bakken changes rapidly both vertically and spatially. Tracking the Middle Bakken is a major challenge for drillers. Improving seismic resolution to better image these complex reservoirs is a key objective of Bakken operators. Because resolution is interplay of both vertical and spatial samplings, and intra-array statics plays an important role in resolution (Egan et al., 2010), both must be considered in improving the resolution. Conventional seismic acquisition and processing focuses on vertical sampling and ignores the spatial sampling. This puts the conventional seismic at an inherent disadvantage with respect to the point-receiver acquisition and processing system in resolving thin beds. This is exemplified in the present paper through processing a dense point-receiver data set acquired over the Williston Basin in North Dakota, where the exploration and production target is the Middle Bakken. We found appreciable improvement in signal-to-noise ratio and usable bandwidth in the point-receiver data compared to that in the conventional data. The ability of statics correction before digital-group-forming (DGF) helps significantly in this regard. The large channel counts in point-receiver data also improve the signal-to-noise ratio and usable band width. These are reflected in the final acoustic impedance inversion results.

Introduction

Recent integrated reservoir characterization studies (Theloy, 2011) reveal the very heterogeneous nature of shale reservoirs. The heterogeneity is in lithofacies and texture of rocks, petrophysical and petrochemical properties, mechanical properties, and other properties. These properties can be conveniently grouped into two main categories: reservoir quality (RQ) and completion quality (CQ). We define reservoir quality primarily by the volume of hydrocarbons within the shale matrix and the permeability of this matrix. Shale has to contain adequate volumes of hydrocarbons that can flow to created hydraulic fractures. The hydrocarbon in place is a function of effective porosity, hydrocarbon saturation,

pore pressure and thickness. Completion quality has to do with the ability to generate and sustain a conductive hydraulic fracture so that hydrocarbons will flow from the matrix to the wellbore at economic rates. This is a function of the state of stress in the formation and fracture complexity. Complexity is impacted by the presence, orientation, and morphology of natural fractures plus the anisotropy of the stress field.

A well is successful when it lands in a zone with good reservoir quality and good completion quality. Effective hydraulic fracture can be initiated in such zones and then grow into larger zones. Table 1 provides a list of RQ properties for three major shale basins in the USA.

The Williston Basin is a large sedimentary basin situated approximately in the middle of the North American continent. The basin, which covers parts of Montana, North Dakota, and South Dakota (Figure 1), contains the largest undeveloped oil play in the USA. It also extends into the southern Saskatchewan region of Canada.

The Bakken resource resides in complex shale reservoirs containing interbedded sands, silts, dolomites and limestones of the upper Devonian and the lower Mississippian age at depths ranging from about 7,000-10,000 ft (2,150-3,050 m). Oil is produced from several levels, but the most notable reservoir is a dolomite layer that resides within the Middle Bakken Shale Formation. The Middle Bakken (Figure 2) is usually of the order of 50 ft (15 m) thick, and the dolomite layer is considerably thinner. The matrix permeability is typically low; however, optimally placed horizontal wells can intersect natural fractures that provide conduits for the oil. Artificial (hydraulic) fracturing is applied to create new fractures and widen natural fractures around a well.

The pay zone is highly heterogeneous, with lithology changing rapidly both vertically and laterally. These variations are often at sub-seismic scale, so despite the fact that overall seismic data quality has historically been considered to be fairly good in the Williston Basin, improving resolution is one of the industry's key objectives. Most efforts to date have concentrated on improving temporal resolution; however, lateral resolution is also important for identifying the spatial extent of reservoirs. Indeed, as discussed by Egan et al. (2010), and El-Kaseeh et al. (2010), lateral resolution and temporal resolution are closely interrelated.

The key objectives of the seismic feasibility tests in the Williston Basin were to investigate the extent that point-receiver acquisition, combined with a broadband seismic source, broadband receivers, and modern data processing algorithms, could improve temporal and lateral resolution relative to conventional acquisition systems. Previous work (Banik et al., 2010) did not provide a direct comparison between conventional and point-receiver data shot in the same area and processed with the same modern processing methods.

Two important factors for resolution in conventional system are intra-array statics and intra-array moveout. Egan et al. (2010), showed the resulting degradation (Figure 14 of the Egan et al., 2010) of the signal amplitude spectra with increasing array size through synthetic calculation of the effects. Another critical factor discussed is sparse common midpoint (CMP) binning. In this article we used densely spaced point-receiver data to simulate the conventional geometry, and process the raw simulated conventional data and the raw point-receiver data following the same workflow but with appropriate processing parameters. This enabled us to directly compare the qualities of the two data sets shot over the same area. We do this comparison in the post-migration prestack and poststack domains. Acoustic impedance products of the two data sets were also compared against the well acoustic impedance profile.

Seismic Data

A summary of the data acquisition parameters is given in Table 2. A detailed description can be found in Egan et al. (2010). The broadband seismic signal was recorded by geophone accelerometers (GACs). The GACs were deployed closely spaced (10 ft, 3.28 m) with the data from each accelerometer recorded as a separate trace. The accelerometers were laid out in an inline quasi-linear fashion. Oversampling enabled us to conduct the current decimation test. Dense sampling of point-receiver data enables a wide variety of noise types (including, for example, ground roll) to be effectively attenuated by data processing algorithms. At the time, a single sweep at each shot-point location was considered adequate. The shot points were parallel and close to the geophone line. The spacing was 100 ft (30.5 m).

Conventional seismic surveys are acquired with arrays of geophones hard-wired together to provide one recorded trace. Usually, there are six geophones in an array. The outputs of these geophones are summed together. This is a simple and robust way of reducing random noise, but can severely impact the quality of the recorded signal. Intra-array statics — variations in the time of a reflection between one geophone to the next — may substantially degrade the signal. The first stages of the processing sequence for point-receiver data are designed to address these static variations. In conventional 2D line acquisition, the shot-point spacing could be 200 ft (61 m) or more and the geophone-group spacing is 160-200 ft. (50- 61 m). In simulating the conventional acquisition, we disregarded every other shot gather and group-summed six adjacent geophones, discarding 14 traces at the end of each group. No additional processing of point-receiver data was applied before summing or discarding the traces. Thus the nominal CMP bin spacing of the simulated conventional data was 100 ft (or 30.5 m). All processing, including isotropic and anisotropic curved-ray prestack time migration (PSTM), of these conventional data was conducted at this 100 ft (30.5 m) grid spacing.

In processing the point-receiver data, we maintained the point-receiver spacing throughout the static application and noise reduction. Just before conducting PSTM, we group-formed point-receiver data combining four geophones. A special summing algorithm in the time-frequency domain was applied to reduce random noise in data. The nominal CMP binning of this data set during and after migration was 20 ft (6.1 m). Common processing steps for both data sets are shown in Figure 3. Processing parameters were adjusted based on CMP spacing of the data sets. Post-migration processing was kept to a minimum to examine the differences in the two data sets right after migration. Since the area is known to have high vertical transverse isotropy (VTI) anisotropy, especially in the overburden of the Bakken Formation, we also used an anisotropic migration on both data sets.

Results and Discussion

The top panel of Figure 4 shows a window from an example point-receiver shot record that captures the main targets of interest – including the Middle Bakken. A time-dependent gain function was applied to compensate for geometrical spreading losses, but otherwise this is a raw record. Undulations in the reflection curves clearly show the presence of near-surface static anomalies. Indeed, some of the undulations have wavelengths that are almost as short as group spacing used in conventional surveys, which are typically 165-220 ft (50-67 m). The times of the point-receiver first breaks were automatically picked and after proper quality checks, fed into a refraction statics program. The bottom panel of Figure 4 shows the same record after application of static corrections to the point-receiver data.

Group forming without intra-array corrections was applied to simulate shot records from the acquisition geometry with 200 ft (61 m) receiver group spacing. Tomographic refraction statics calculated from point receiver data were applied to simulated conventional data at the appropriate CMP locations after group forming. In the case of point-receiver data the refraction statics was applied right after geometry update and datum correction. In creating the 20-ft (6.1 m) CMP bins for point receiver data, we applied timefrequency — diversity sum‖ of four point receiver traces, just before the final migration. Otherwise, all processing steps listed in Figure 3 were appropriately applied to both data sets.

After migration, all of the traces within each record were stacked using a mute function selected from the real data. Note that this mute was tight enough to prevent normal move-out (NMO) stretch from being a significant factor in the subsequent frequency analysis. Figure 5 shows the stack sections of both data sets after migration. The signal and noise spectra of the stacked data are shown in Figure 6. It is clear that point-receiver data provide uplift in signal/noise amplitude spectra compared to those of the conventional data. The bandwidth is more flat and the difference between signal and noise is at least three times more up to 100 Hz. The usable maximum frequency in this case, without further sigal-to-noise (S/N) enhancement, is 60 Hz. For additional bandwidth enhancement, which may be necessary to resolve thin beds, the point-receiver data will be more suitable than the conventional data. A high channel count due to dense receiver and shot spacing in the point-receiver data is definitely a factor for improved (S/N), but accounting for statics and move-out before group forming are significant contributing factors. We have verified that if intra-array statics and intra-array move-out are not addressed, they rob considerable frequency content from the final stacked trace. The sharp reduction in signal from 20 Hz to 60 Hz in the simulated conventional data (Figure 6) is due to this intra-array statics.

The improved signal-noise spectra in the point receiver data is reflected in the quality of the inverted acoustic impedance seismic well ties; this is shown in Figure 7. In Figure 8 we show the inverted acoustic impedance profiles at three well locations with varying production history. In Figure 8a, point-receiver acquisition and processing were applied, while in Figure 7b the conventional data was used. We note the spatial variability in point-receiver data, while no such variability is seen in conventional data. The spatial variability seen in Figure 8a is consistent with the production history of the three wells. In Figure 9, we show the well tie after we applied a spectral-whitening process to the point-receiver data, raising the maximum frequency to about 90 Hz. The Bakken Formation is more clearly seen in the inverted impedance profile (blue curve) and it matches quite well with that measured from well data (red curve). The stack section and the corresponding signal and noise spectrum of the spectrally whitened stack data is shown in Figure 10. The noise level in the simulated conventional data did not allow application of the spectral whitening process.

Conclusion

The objectives of this study were to examine the potential benefits of dense point receiver acquisition for reservoir characterization in the Williston Basin and compare the results directly with conventional data shot in the same area. Because of the dense acquisition geometry, we could decimate the data to simulate the conventional geometry in the area and process the two data sets using the same modern processing steps. We report that dense-point receiver data provide significant improvements in signal-noise bandwidth, and consequently improved resolution and reservoir characterization products. A significant part of this improvement comes from the ability to process data before statics removal. Dense spatial sampling helps improve vertical resolution as well.

Acknowledgment

We appreciate the encouragement provided by Schlumberger-WesternGeco management in completing this work.

References Cited

Banik, N., A. Koesoemadinata, and G. El-Kaseeh, 2010, Young's modulus from single-sensor surface seismic data: 80th SEG International Annual Conference, Denver, Colorado.

Egan, M.S., J. Seissiger, A. Salama, and G. El-Kaseeh, 2010, The influence of spatial sampling on resolution: CSEG Recorder Focus Article, p. 30-36.

El-Kaseeh, G., N. Banik, A. Koesoemadinata, M., Egan, and A. Salama, 2010, Seismic feasibility tests in the Williston Basin to improve reservoir characterization: First Break, v. 28/6, p. 91-95.

Le Fever, J.A., C.D. Martinuik, and P.A. Mahnic, 1991, Petroleum potential of the Middle Member, Bakken Formation, Williston Basin, Proceedings of the Sixth International Williston Basin Symposium: Sakatchewan Geological Society Special Publication 11, p. 76-94.

Theloy, C., 2011, Integrated rock mechanics and natural fracture study on the Bakken Formation, North Dakota: Bakken Consortium meeting, December 2, NETL-DOE sponsored research, Geology and Geological Engineering, Colorado School of Mines, Golden, Colorado.

Figure 1. Location of the Williston Basin.

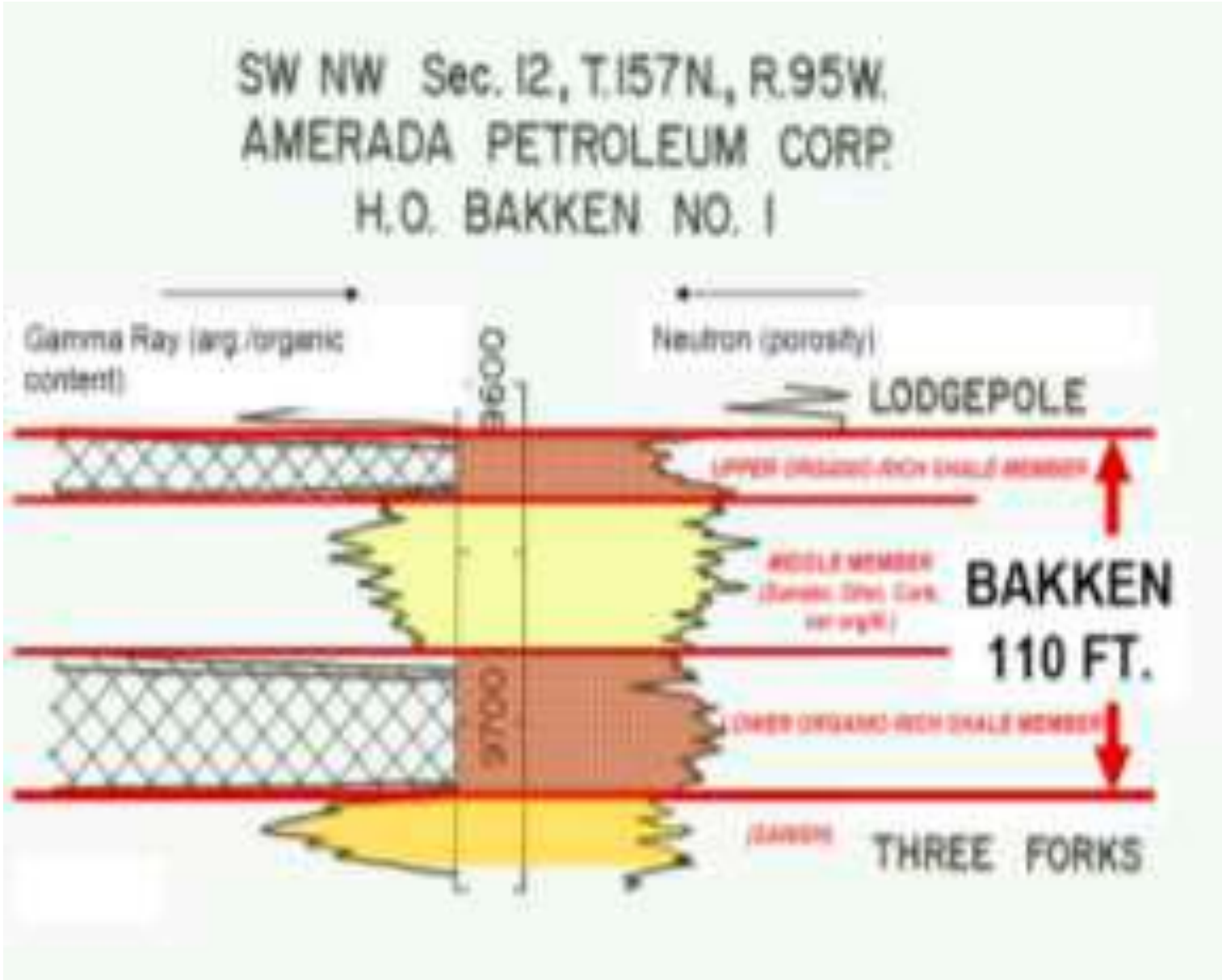

Figure 2. Typical Bakken Formation in North Dakota and Montana. Source: www.searchanddiscovery.com.

Figure 3. Common processing steps for two.

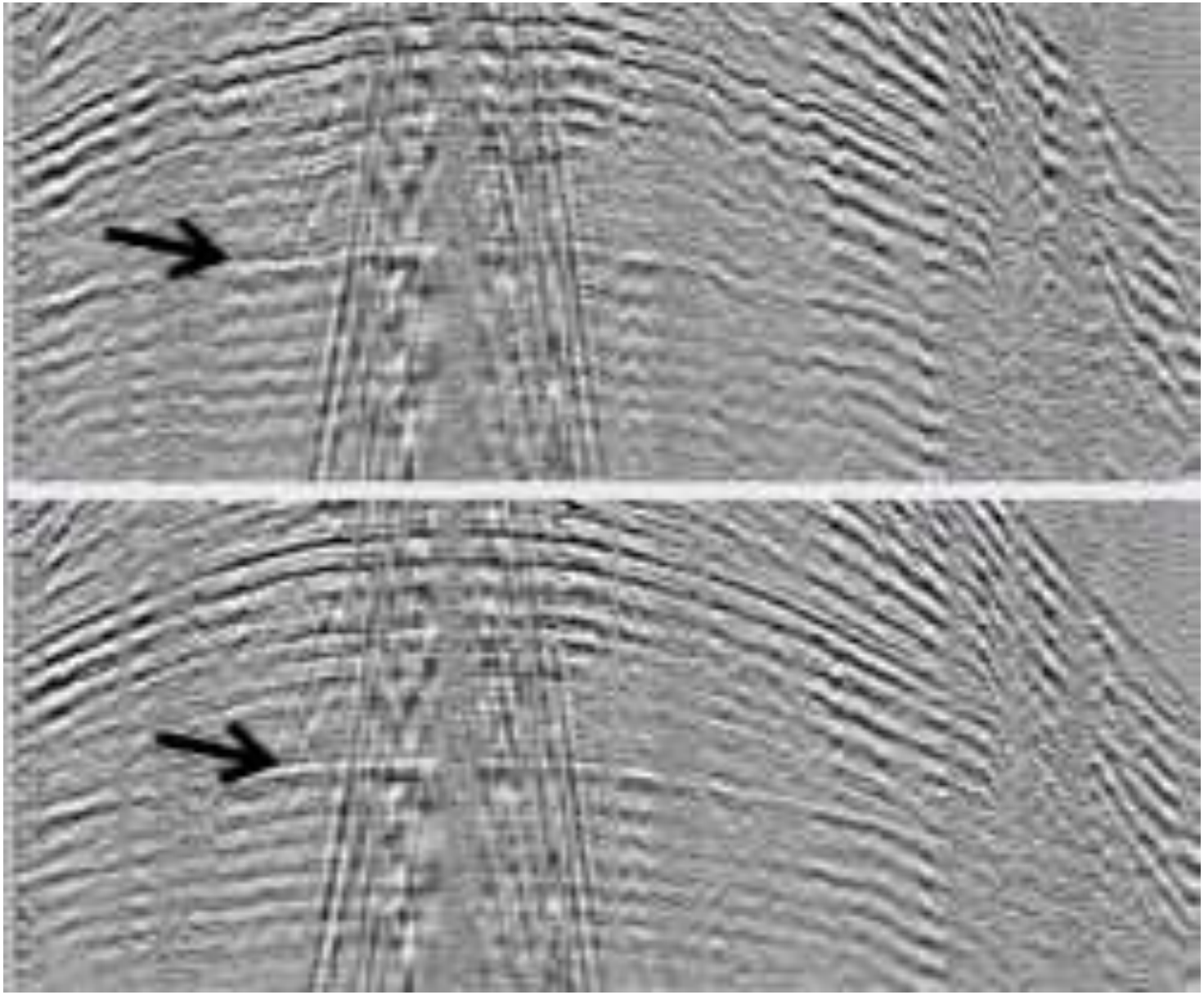

Figure 4. Example of a point receiver shot gather data sets. windowed to include the Bakken reflection.

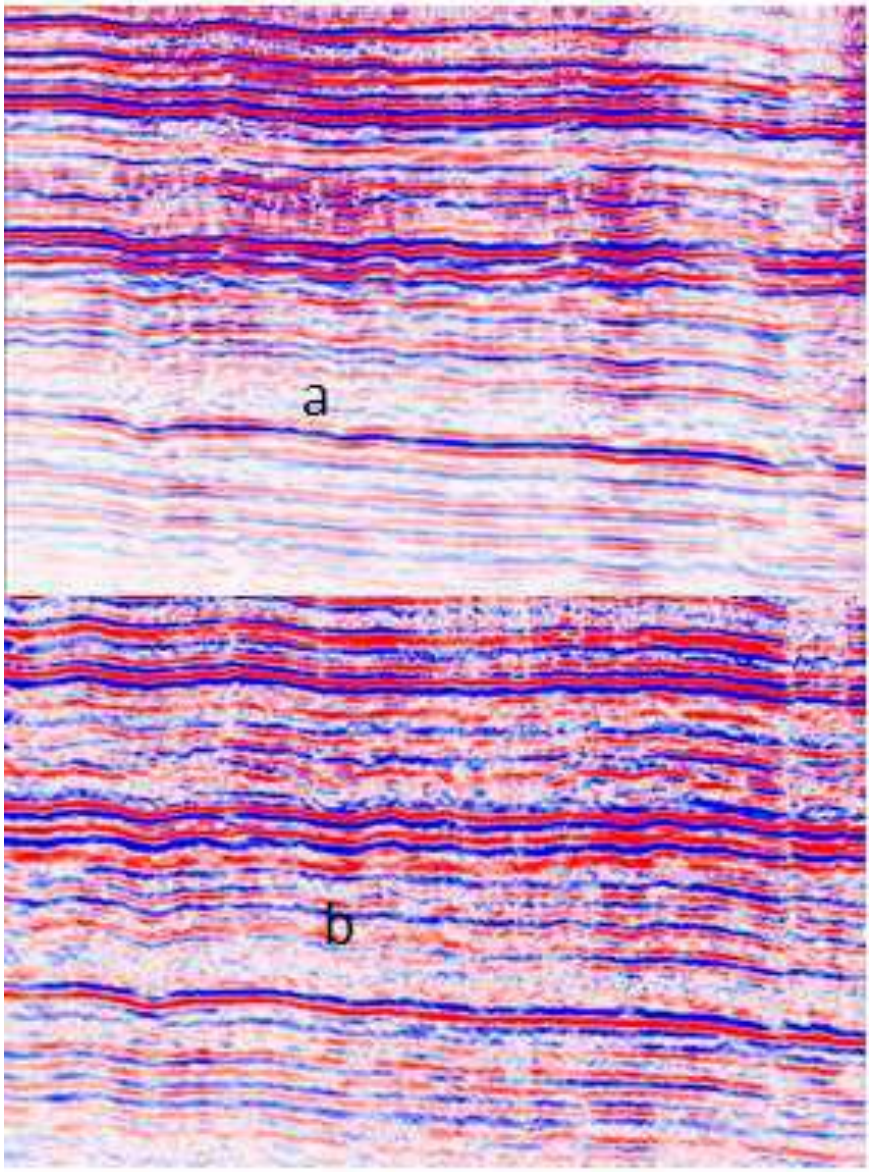

Figure 5. Post-migration stacks for (a) point-receiver data and (b) simulated conventional data.

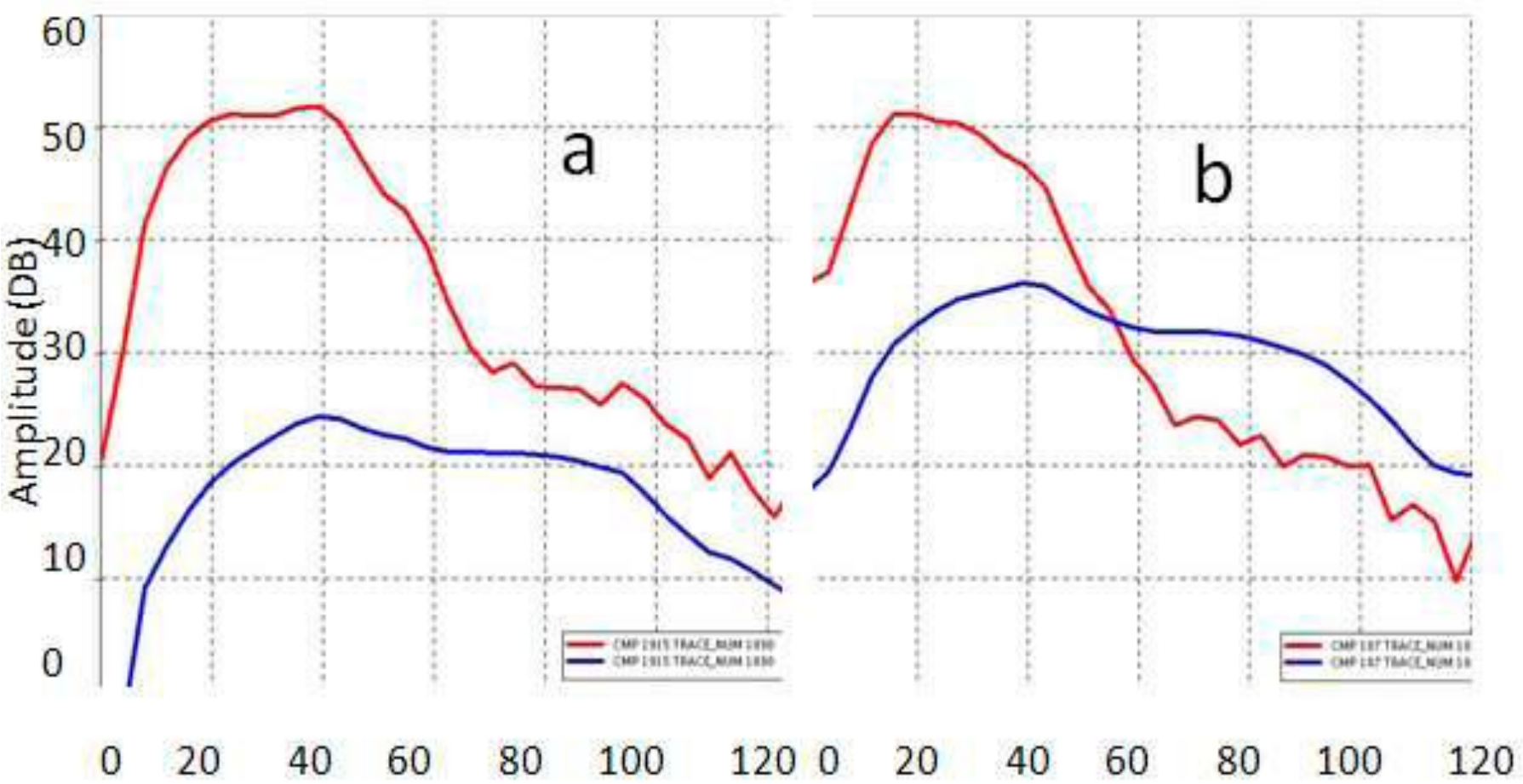

Figure 6. Signal (red) and noise (blue) spectra of point-receiver (left) and simulated conventional data (right).

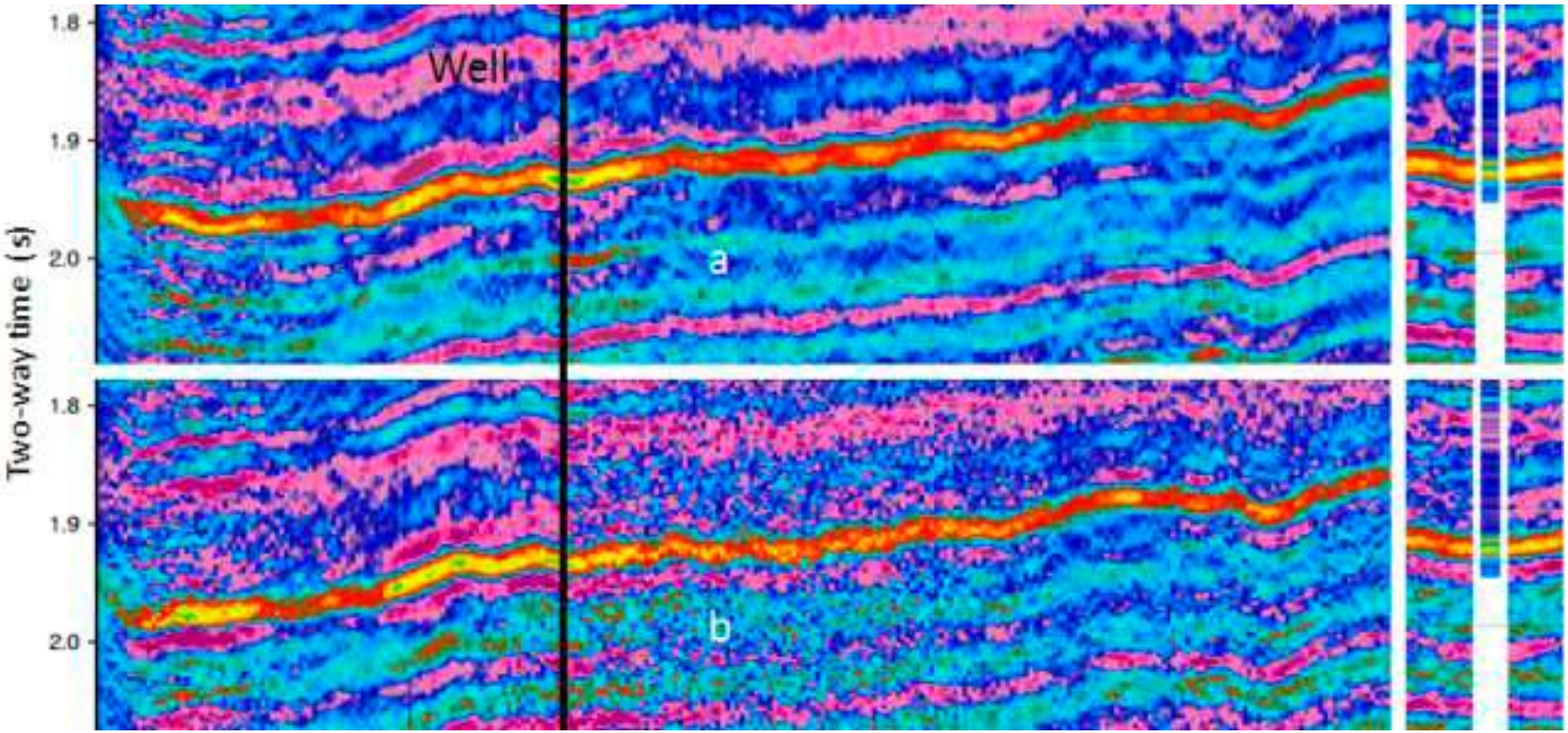

Figure 7. Inverted acoustic impedance section for point-receiver data (top) and conventional data (bottom). The Bakken formation is seen in red and yellow colored layer. Corresponding well ties are shown on the right. The well location is marked by the black line.

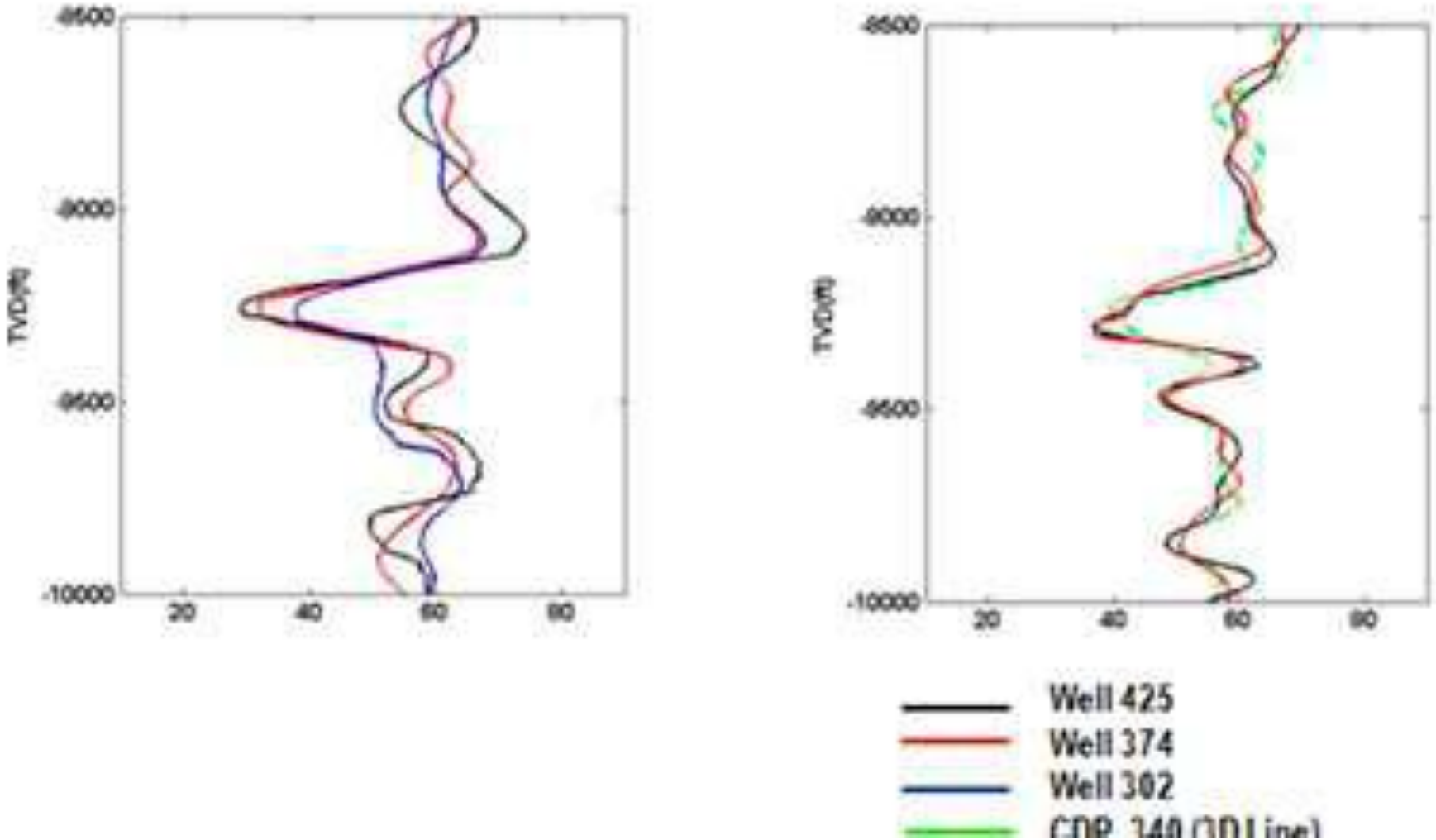

Figure 8. (Left) Point-receiver and Young's modulus at three different locations on the 2D line and (right) the same for conventional data.

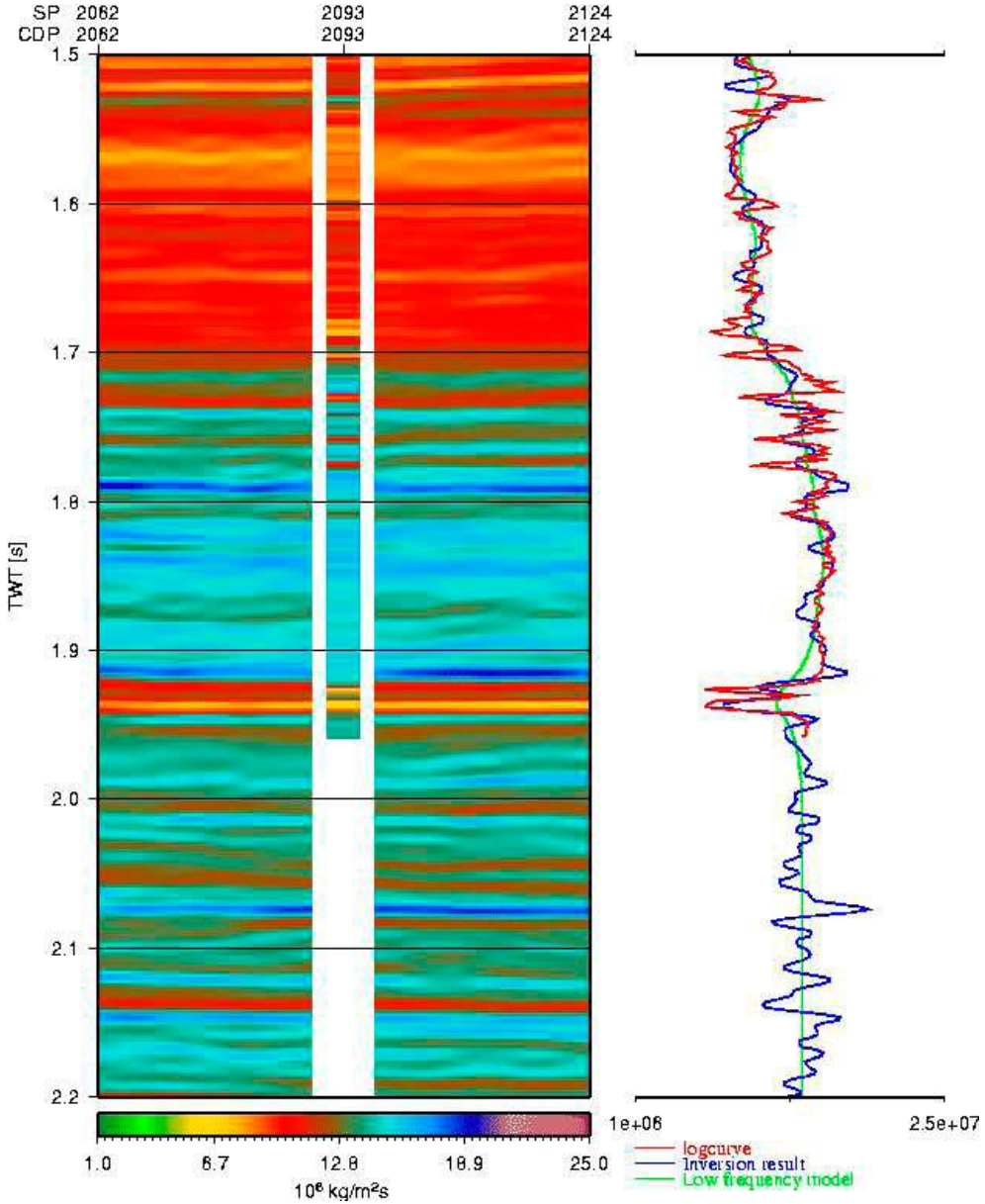

Figure 9. Well-tie comparing the well Young's modulus (red) with the point-receiver seismic Young's modulus (blue) at the well location. The point-receiver seismic data has been whitened to 90 Hz as discussed in the text.

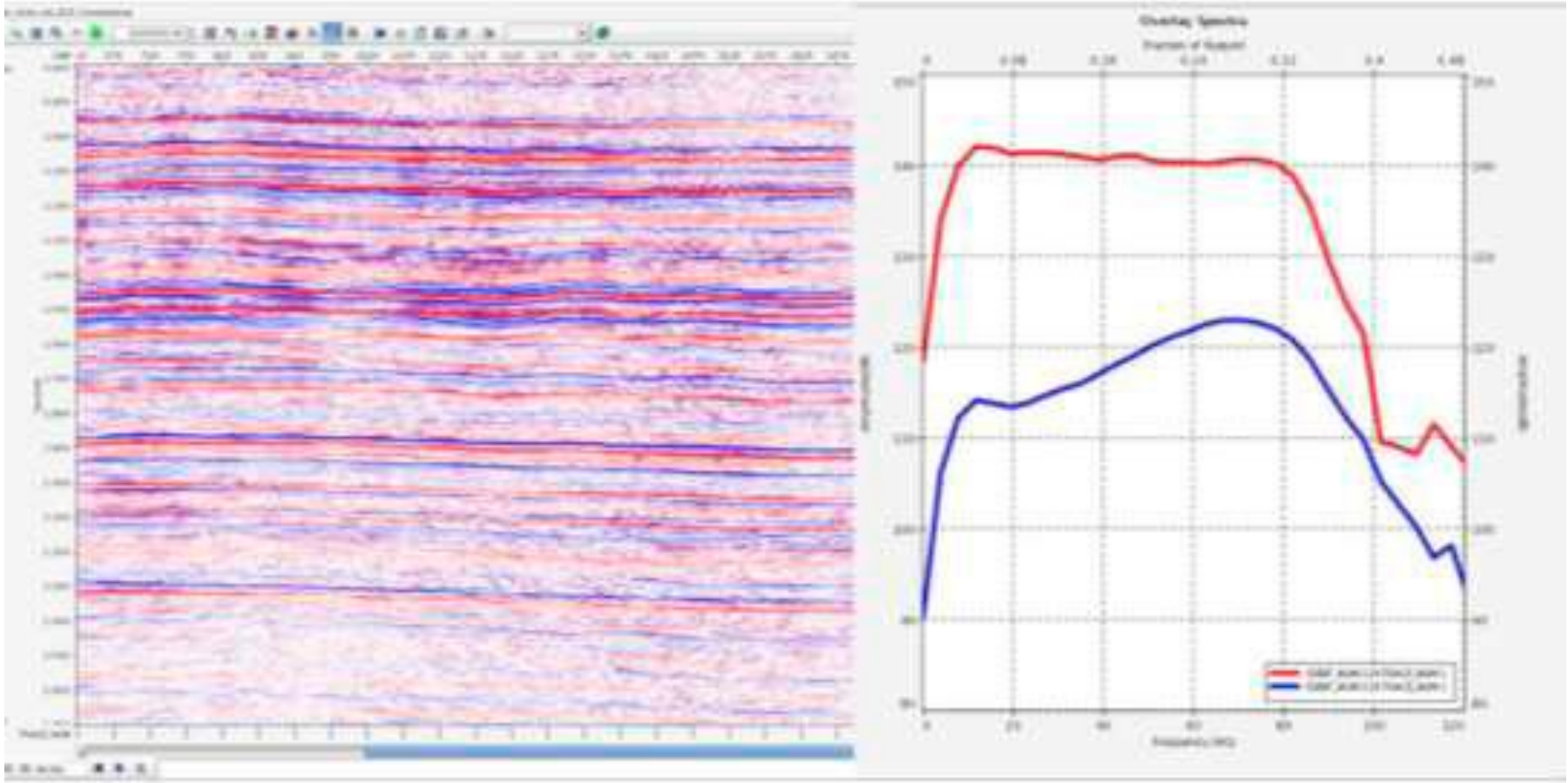

Figure 10. Spectrally whitened stack section and the corresponding signal and noise spectra.

Source Point Interval	100 feet
Source line length	12 miles
Spread type	Symmetrical split-spread
Inline Single Sensor Interval	10 feet
Minimum Offset	5 feet
Maximum Offset	20,040 feet
Recording Instrument	Q-Land MAS
Sample Interval	2 msec.
Total live channels	4,008
Sensor type	Geophone Accelerometer (GAC)
Source Type	Vibrators
Starting frequency	4 Hz
Ending frequency	120 Hz
Listening time	5 sec.
Sweep type	Maximum Displacement (MD) Sweep
Number of sweeps per VP	1
Number of vibrators per group	3
Nominal array	Inline – bumper to bumper

Table 1. Average reservoir properties of three shale basins in the USA.

Basin	Haynesville	Marcellus	Bakken
Age (MYA)	170	385	350
Lithology	Argillaceous	Argillaceous	sand-/silt stone/carbonite
Total Area	9,000	95,000	200,000
Total Gas (tcf)	717	1,500	485.1
Producable Gas	251	356	20.66
GIP (bcf/sq mi)	175	200	28.3
Av. Depth (ft)	12,000	7,000	10,000
Thickness (ft)	225	350	150
Average EUR	6.5	4	1.41
Pressure (psi)	8,500	4,000	5,600
Temperature (F)	340	130	140
BO	2.2	1	1
TOC (%)	3	3	10
Porosity (%)	8	8	5
Matrix permeability	658	1,000	
Clay Content (%)	27	50	10,000
silica/carbonate/calc	53	30	5
Adsorbed gas (%)	18	50	95
Average IP	10		0

Table 2. Data acquisition parameters for the test Line.